RESEARCH ARTICLE

Macromolecular Chemistry and Physics
www.mcp-journal.de

Imperfect Crystals of Poly(butylene succinate) Formed at High Supercooling of the Melt

*Katalee Jariyavidyanont, Xiaoshi Zhang, Christoph Schick, Alicyn M. Rhoades, and René Androsch**

Prior work revealed distinct differences in the X-ray diffraction patterns of poly(butylene succinate) (PBS) melt-crystallized at different temperatures, regarding the number, width, and position of diffraction peaks, detected in isotropic samples. To further evaluate whether the observed differences are caused by a change of the unit cell, or are solely due to different crystal sizes and perfection, X-ray fiber patterns of solid-state oriented PBS are acquired and analyzed. The data reveal that PBS crystallized at high supercooling of the melt at 20 °C contains crystals with enlarged dimensions of the monoclinic unit cell in the cross-chain direction, compared to PBS crystals initially grown at 20 °C and subsequently reorganized at elevated temperature at 100 °C. High-temperature reorganized crystals exhibit a unit cell similar to that formed after direct crystallization of the quiescent melt at the same high temperature, with the latter, however, unable to draw for observing X-ray fiber pattern. The observed changes in the unit cell of PBS when changing the crystallization temperature are discussed in the context of the widely observed crystallization-temperature-induced crystal polymorphism in other polymers.

1. Introduction

Poly(butylene succinate) (PBS) is a crystallizable linear polyester of increasing economic importance related, among others, to its biodegradability and the possibility for synthesis based on short-term renewable resources, offering application as packaging material, in agriculture, or in the biomedical sector.[1–5] However, the required properties crucially depend on the presence of crystals due to the low glass transition temperature of ≈−35 °C.[6–9] Crystallization of PBS at low supercooling of melt below the equilibrium melting temperature of ≈130 °C[8–12] proceeds by spherulitic growth of relatively thin lamellae,[11,13–17] starting from a few heterogeneous nuclei, and with the size of crystals and spherulites decreasing with increasing melt-supercooling.[18] Eventually, on crystallization near the glass transition temperature, spherulites with an inherent radial symmetry are absent, likely related to the high number of homogeneous nuclei.[18] In addition to the changes in the crystal morphology and their superstructure, detected by microscopy and small-angle X-ray scattering (SAXS), a distinct dependence of the X-ray diffraction (XRD) patterns on the crystallization temperature is observed.[12,18,19] Qualitatively, XRD peaks obtained on isotropic samples, measured at an identical reference temperature, broaden, merge, and/or shift to lower scattering angles on decreasing the crystallization temperature, or even seem to completely disappear when being low in intensity. These observations typically point to the formation/presence of small and defective crystals,[20] however, with the determination of unit cell parameters obscured due to frequent superposition of scattering contributions from different lattice planes.

Regarding the crystal structure, PBS is polymorphic and shows a stress-induced (reversible) crystal transformation. In the absence of stress, molecular segments arrange in the α-phase, while above a critical stress of 140 MPa, α-crystals transform to β-crystals, involving a change from a non-planar to an extended all-*trans* chain conformation of the tetramethylene unit. In both α- and β-crystals, the unit cell is body-centered monoclinic, containing two chain repeat units.[13,21–23] Crystal structure analyses were based on uniaxially oriented fibers prepared by melt-spinning at 200 °C, followed by additional drawing and annealing at 80 °C,[21–23] or on cast films prepared from a solution and stretched at 80 °C.[13] However, a systematic evaluation of the effect of the crystallization/annealing temperature has not been performed, and therefore no information about the possible influence of melt-crystallization conditions on the

---

K. Jariyavidyanont, R. Androsch
Interdisciplinary Center for Transfer-oriented Research in Natural Sciences (IWE TFN)
Martin Luther University Halle-Wittenberg
06099 Halle/Saale, Germany
E-mail: rene.androsch@iw.uni-halle.de

X. Zhang, A. M. Rhoades
Plastics Engineering Technology & Polymer Engineering and Science
Penn State Behrend
5101 Jordan Rd, Erie, PA 16563, USA

C. Schick
University of Rostock
Institute of Physics & Competence Centre °CALOR
18051 Rostock, Germany

The ORCID identification number(s) for the author(s) of this article can be found under https://doi.org/10.1002/macp.202500079

© 2025 The Author(s). Macromolecular Chemistry and Physics published by Wiley-VCH GmbH. This is an open access article under the terms of the Creative Commons Attribution License, which permits use, distribution and reproduction in any medium, provided the original work is properly cited.

DOI: 10.1002/macp.202500079

crystal structure of PBS is available. Such investigation, however, seems important as the formation of different crystal polymorphs on crystallizing the isotropic and relaxed melt at different temperatures has been proven for many crystallizable polymers. Often non-equilibrium—though in certain temperature ranges metastable—conformationally disordered crystals or mesophases grow at rather high supercooling of the melt, in contrast to the formation of more perfect crystals at relatively high temperatures. Prominent examples include isotactic polypropylene (iPP),[24,25] polyamides (PA),[26–29] or poly(L-lactic acid) (PLLA),[30,31] with the presence of different polymorphs then also affecting ultimate, for example, mechanical properties.[32–36] However, worth noting, crystallization-temperature-controlled crystal polymorphism is not a general observation as there is a similarly large number of polymers for which the crystallization temperature seems of low importance regarding the formation of different crystal structures, e.g. poly(butylene terephthalate).[37]

In order to advance the present incomplete knowledge of the crystal structure of PBS formed at low temperatures, samples were crystallized at 20 °C and then uniaxially oriented before observing X-ray fiber patterns of the resulting small and, presumably, defective crystals. Afterward, the samples were annealed at 100 °C, allowing distinct crystal reorganization, before remeasurement of the X-ray fiber patterns and analysis of changes in the unit cell. Note again that in prior experiments a similar thermal profile was applied for analysis of isotropic samples,[19] which, however, did not yield unambiguous outcomes.

2. Materials and Instrumentation

The study was performed on an extrusion-grade PBS with a mass-average molar mass of 123 kg mol^{-1}, obtained from MCPP Germany GmbH in the form of pellets.[38,39] The material was processed by compression molding to films with a thickness of $\approx$200 μm, involving a final quenching step employing water with a temperature of 20 °C as coolant, to ensure isothermal low-temperature crystallization. From the obtained circular films, mini-tensile bars were punched out and subjected to tensile deformation using a homemade stretching device until a local strain of $\approx$400 %, estimated by marks in the center of the specimen, was achieved. Afterward, the sample was unclamped from the stretching device and allowed to relax, before X-ray analysis.

XRD experiments were performed in transmission mode employing a Retro-F laboratory setup (SAXSLAB, Copenhagen, Denmark) in combination with a microfocus X-ray source (AXO Dresden GmbH, Dresden, Germany) and an ASTIX multilayer X-ray optics (AXO Dresden GmbH) for monochromatization. We used CuKα radiation with a wavelength λ of 0.154 nm, and the approximately circular beam had a size of $\approx$0.5 mm. The scattered X-ray intensity was detected with a flat 2D-PILATUS3 R 300K detector (DECTRIS Ltd., Baden, Switzerland), and plotted vs the scattering vector $q = \frac{4\pi}{\lambda}\sin\theta$, with θ being the Bragg angle. The sample-detector distance of $\approx$87 mm was calibrated using silver behenate. In order to expand the limited observable q-range, the detector was positioned asymmetrically with respect to the primary beam. The uniaxially drawn samples were positioned on the silver block of an HFS350 hot stage (Linkam, Tadworth, UK), serving as a sample holder and containing a hole with a diameter of 1 mm for passing the X-rays. First, the fiber pattern of the drawn and relaxed sample—crystallized at 20 °C and not further thermally treated—was recorded. Then, the sample was annealed at elevated temperature by heating to 100 °C using the sample-holder hot stage, followed by immediate re-cooling to 20 °C and repeated collection of the X-ray fiber pattern. Worth noting that distinct shrinkage on heating the stretched samples was not observed.

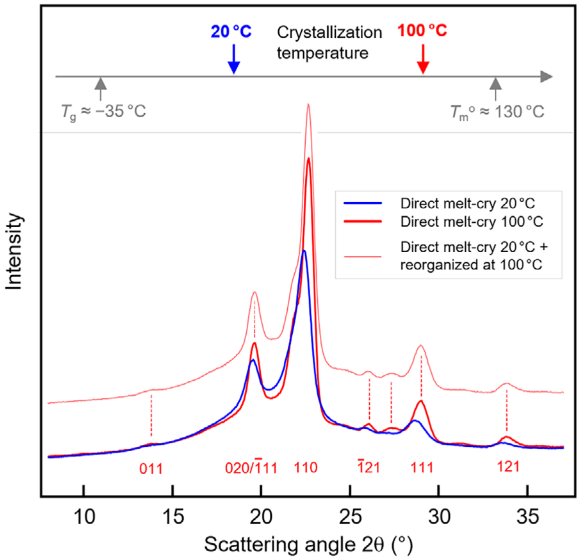

Figure 1. XRD curves of isotropic films of PBS melt-crystallized at 20 °C (blue) and 100 °C (red), with the crystallization temperature directly approached by fast cooling the equilibrium melt, denoted "Direct melt-cry" in the legend. The light-red curve represents the XRD pattern of a sample which initially was melt-crystallized at 20 °C and subsequently reorganized by heating to 100 °C. All measurements were performed at room temperature. Selected peaks are indexed based on crystal-structure information from the literature.[21] The upper panel scales the crystallization temperature relative to the equilibrium melting temperature T_m^o and glass transition temperature T_g, illustrating the different supercooling of the melt during crystallization. XRD data of non-reorganized PBS are adapted under terms of the CC-BY license 4.0 (https://creativecommons.org/licenses/by/4.0/), Copyright 2023, from R. Androsch, K. Jariyavidyanont, A. Janke, C. Schick, published by Elsevier (https://doi.org/10.1016/j.polymer.2023.126311).

3. Results and Discussion

For an illustration of the scope of the present study, **Figure 1** shows XRD curves of isotropic films of PBS melt-crystallized at 20 °C (blue) and 100 °C (red), with selected diffraction peaks indexed based on crystal-structure information from the literature.[21] Crystallization at 100 and 20 °C corresponds to supercooling of the melt of $\approx$30 and 110 K, respectively, as is schematically shown with the temperature scale in the upper part of the plot. In both cases, crystallization at 20 and 100 °C, semicrystalline structures containing 30%–35% crystal lamellae with thicknesses of $\approx$4 and 6 nm, respectively, are obtained.[18] A comparison of the X-ray patterns reveals that in the case of crystallization at 100 °C, the number, width, and position of peaks may be different than after crystallization at 20 °C. Though it appears that after low-temperature crystallization some peaks are no longer detectable, became much broader, or shifted to lower

© 2025 The Author(s). Macromolecular Chemistry and Physics published by Wiley-VCH GmbH

15213935, 2025, 11, Downloaded from https://onlinelibrary.wiley.com/doi/10.1002/macp.202500079 by Martin Luther University Halle-Wittenberg, Wiley Online Library on [27/06/2025]. See the Terms and Conditions (https://onlinelibrary.wiley.com/terms-and-conditions) on Wiley Online Library for rules of use; OA articles are governed by the applicable Creative Commons License

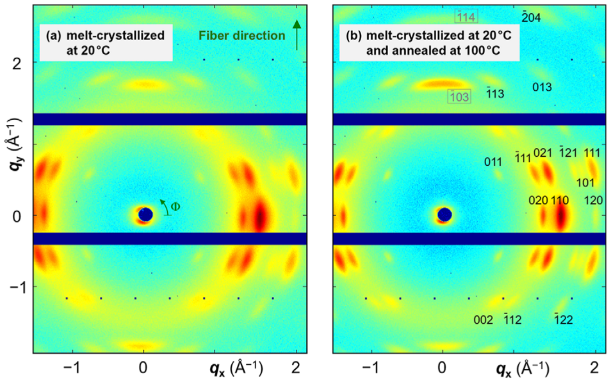

Figure 2. XRD fiber patterns of PBS. The left image a) was collected after melt-crystallization at 20 °C, with the initially isotropic film uniaxially stretched by ≈400 % at room temperature, followed by relaxation. Image b) to the right was observed after additional heating to 100 °C, to allow crystal reorganization. The fiber direction and definition of the azimuthal angle Φ are indicated in the left image. Indexing of scattering maxima is based on the literature,[21] with further explanations provided in the text.

scattering angles, potentially indicating a larger unit cell than after high-temperature crystallization, a final interpretation of the origin of these observations is impossible without further experimentation. In particular, conclusions about whether low-temperature crystallization is connected with qualitative and/or quantitative changes of the unit cell, to be discussed in terms of incorporation of conformational defects into the crystals, cannot yet be drawn. In addition, Figure 1 shows with the light-red curve the XRD pattern of a sample which initially was melt-crystallized at 20 °C and subsequently reorganized by heating to 100 °C. This pattern reveals an identical crystal structure as obtained for PBS directly crystallized from the melt at 100 °C (red curve), as judged by visual inspection of peak positions (see also the dotted vertical lines at selected peaks). This information is important as the X-ray fiber pattern of PBS directly melt-crystallized at 100 °C could not be obtained, in contrast to reorganized samples, as further outlined below.

As an example, **Figure 2** shows with the left image a) the XRD fiber pattern of PBS melt-crystallized at 20 °C. The initially isotropic film —with its azimuthally averaged XRD pattern shown with the blue curve in Figure 1—was uniaxially stretched by ≈400 % at room temperature, and allowed to relax afterward, to avoid/revert stress-induced transformation of the α- into the β-structure.[21–23] Image b) (right) was observed after additional heating to 100 °C, to allow crystal reorganization as described in detail elsewhere.[19] It is important to note that large-strain solid-state deformation of semicrystalline PBS containing crystals grown directly from the quiescent melt at 100 °C, to obtain the corresponding crystal structure, is not possible, likely due to the formation of rather large spherulites, causing brittleness.[40] Such morphology was proven evident in melt-crystallization at relatively high temperatures by independent studies,[13,15,41–43] including the particular PBS grade used in the present work.[18] However, as judged by inspection of XRD data obtained on isotropic PBS directly melt-crystallized at 100 °C on one side, and isotropic PBS melt-crystallized at 20 °C and then reorganized by heating to 100 °C on the other side (see red and light-red curves in Figure 1, respectively), these different nucleation/crystallization pathways seem not to affect the unit cell.

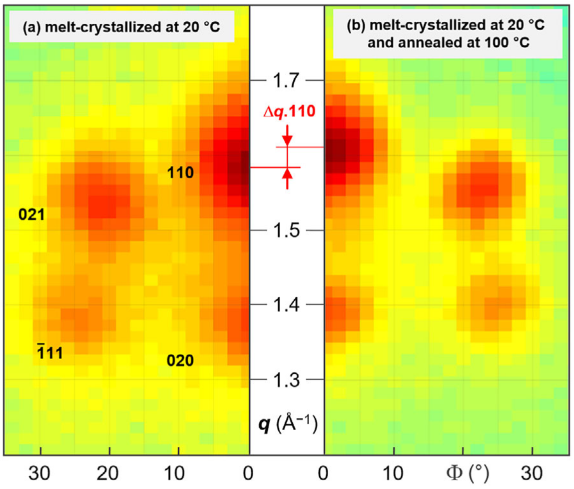

Figure 3. Polar plots of parts of the XRD fiber patterns of Figure 2, that is, of uniaxially drawn PBS melt-crystallized at 20 °C, a) before and b) after annealing/recrystallization by heating to 100 °C, showing the strong zero- and first-layer line peaks at q-values ≈1.5 Å^{-1}, for demonstration of the shift of the 020 and 110 peaks to higher q-values after high-temperature annealing.

Both fiber patterns (Figure 2a,b) show peaks which all are characteristic of the α-structure of PBS, and there is no indication of the presence of β-crystals.[21–23] The crystal orientation, as judged by the azimuthal width of scattering maxima, is lower than that achieved after melt-spinning at 200 °C, drawing at room temperature, and additional annealing at 80 °C, as applied for determination of the crystal structure in the literature.[21] However, the orientation is considered sufficient to analyze the effect of the crystallization temperature on the unit cell. The peaks are aligned at layer lines and are therefore well-resolved to allow analysis of lattice spacings. Indexing of peaks (see Figure 2b) is based on the literature,[21] except for the gray-labeled reflections $\bar{1}03$ and $\bar{1}14$. These assignments are based on references [13] and [23], and on the match between expected and observed lattice spacings, respectively. The most important observation from Figure 2, however, is that the general angular position and number of peaks seem independent of the thermal history. Instead, mainly the radial width of peaks and their exact location are affected by the crystallization temperature. As expected, crystallization at 20 °C yields broader peaks than after high-temperature crystallization/reorganization, due to the formation of smaller crystals,[20] as well as a change of unit cell parameters is expected from visual inspection of peak positions. For demonstration of the latter observation, **Figure 3** shows parts of the XRD patterns of Figure 2a, b in polar coordinates in the q-range from 1.2 to 1.8 Å^{-1}, for direct comparison of the positions of the strong equatorial 110 and 020 peaks. As such, PBS which was melt-crystallized at 20 °C, and subsequently heated to 100 °C, exhibits smaller interplanar spacings compared to non-annealed low-temperature-crystallized PBS.

Measurements as shown in Figure 2 were conducted on two independently prepared samples. For the second sample, XRD patterns were collected such that the fiber direction was oriented

© 2025 The Author(s). Macromolecular Chemistry and Physics published by Wiley-VCH GmbH

15213935, 2025, 11, Downloaded from https://onlinelibrary.wiley.com/doi/10.1002/macp.202500079 by Martin Luther University Halle-Wittenberg, Wiley Online Library on [27/06/2025]. See the Terms and Conditions (https://onlinelibrary.wiley.com/terms-and-conditions) on Wiley Online Library for rules of use; OA articles are governed by the applicable Creative Commons License

15213935, 2025, 11, Downloaded from https://onlinelibrary.wiley.com/doi/10.1002/macp.202500079 by Martin Luther University Halle-Wittenberg, Wiley Online Library on [27/06/2025]. See the Terms and Conditions (https://onlinelibrary.wiley.com/terms-and-conditions) on Wiley Online Library for rules of use; OA articles are governed by the applicable Creative Commons License

Table 1. Unit-cell parameters, including unit-cell volume and crystal density of the α-structure of PBS melt-crystallized at 20 °C, and of PBS melt-crystallized at 20 °C and subsequently reorganized by heating to 100 °C. The right two columns show the changes of the unit cell parameters when crystallizing at 20 °C, compared to high-temperature crystallization at 100 °C, reported in both absolute and percentage units.

Unit cell parameter	Melt-crystallized at 20 °C	Melt-crystallized at 20 °C and heated to 100 °C	Delta-abs[a]	Delta-%[b]
a_0 [Å]	5.26 ± 0.04	5.21 ± 0.03	+0.05	+1.0 %
b_0 [Å]	9.10 ± 0.03	9.08 ± 0.03	+0.02	+0.2 %
c_0 [Å]	10.87 ± 0.02	10.87 ± 0.03	±0.00	±0.0 %
β [°]	123.02 ± 0.14	123.30 ± 0.23	+0.28	+0.2 %
Volume [Å^3]	436.16 ± 0.84	430.01 ± 1.19	+6.15	+1.4 %
Density [g cm^{-3}]	1.310 ± 0.00(3)	1.328 ± 0.00(4)	−0.018	−1.4 %

[a] Delta-abs = (Melt-crystallized at 20 °C) – (Melt-crystallized at 20 °C and heated to 100 °C) [b] Delta-% = Delta-abs / (Melt-crystallized at 20 °C and heated to 100 °C) × 100 %
Data are averages based on the analysis of two independently prepared samples. In the case of sample 1, a single XRD pattern was obtained for each thermal treatment. In the case of sample 2, two patterns were observed for each crystallization history, including a variation of the fiber direction with respect to the x and y detector coordinates. Errors are rounded up.

parallel to both the x and y direction of the detector, allowing the analysis of the 121 peaks at $q \approx 2.35$ Å^{-1}, in addition to those that were indexed in Figure 2b. The fiber pattern and structure analysis are detailed in the supporting information. The analysis included coordinate transformation to account for the flat detector geometry as illustrated in Figure S1 (Supporting Information). A customized interactive diffraction spot selection code was used to identify diffraction spots near the calculated positions (see also Figure S2, Supporting Information). The q-values associated with specific *(hkl)* lattice planes were averaged, and the complete set of q-values extracted from the fiber pattern was used as input for a custom MATLAB-based unit cell parameter fitting code. Unit cell parameters from the literature,[21] as listed in Table S1 (Supporting Information), were used as initial values. All indexed planes were then subjected to least-squares nonlinear refinement. High R^2 values were achieved in all samples studied, indicating good agreement between observed and calculated d-spacing values. Examples of successful fitting results are provided in Tables S2 and S3, and Figure S3 (Supporting Information).

As the main outcome of this study, **Table 1** shows the unit cell parameters, the volume of the unit cell, and the crystal density of PBS melt-crystallized at 20 °C, and of PBS melt-crystallized at 20 °C and subsequently reorganized by melting and melt-recrystallization at 100 °C. As such, we observed that low-temperature crystallization of PBS leads to a significant increase of the area of the a_0-b_0 basal plane, while the fiber-repeat distance remains unchanged, compared to the unit cell of PBS annealed/recrystallized at high temperature. Ultimately, this causes an increase in the unit-cell volume and a decrease in the crystal density. These are in line with our expectations as low-temperature crystallization may cause entrapment of (conformational) crystal defects, leading to an increase in the distance between neighbored molecular segments due to deteriorated lateral packing. Such behavior, to name only a few examples, has been observed a long time ago for iPP,[24,25] the entire family of aliphatic PAs,[26–29] or, more recently, for PLLA.[30,31] In these cases (iPP, PAs, PLLA), the crystal structures observed during low-temperature crystallization are suggested to be new polymorphs (e.g. the smectic/mesophase structure of iPP,[24,25] the pseudohexagonal mesophase in PAs,[26–29,44] or the disorder α'-phase of PLLA[30,31]). Similar to PBS, these low-temperature-generated structures appear to be metastable within a certain temperature range, may improve their structures within limits by annealing and local-melting-based reorganization, and transform to more perfect crystals only at high temperatures by reorganization at the global scale, with the latter impacting the crystal morphology and lamellar-stack structure. All these features are recognizable by calorimetry, for example by observation of a small but distinct exothermic peak prior to final melting (see the examples of iPP,[45–47] PLLA,[48,49] and PBS[19]). Also common for these examples, the disordered crystals/mesophases typically exhibit a lower bulk enthalpy of melting than the high-temperature-grown counterparts (see iPP,[45,47] PLLA,[50–53] and PA 6[54]), however, quantitative information for the disordered PBS phase is not yet available. As we do not see a qualitatively different crystal structure in PBS crystallized at low temperature compared to high-temperature crystallization, but only an enlarged unit cell, its low-temperature crystal form may not be considered as a specific crystal polymorph, though there are many similarities—e.g. regarding thermodynamic metastability and structural features—to the well-accepted low-temperature-formed polymorphs described above.

4. Conclusion

In this study, we investigated the effect of the temperature of melt-crystallization on the crystal structure of poly(butylene succinate) (PBS). Early X-ray diffraction analyses of isotropic samples containing crystals grown at different supercooling of the melt indicated the formation of crystals of different sizes and perfection, however, without information about the unit cell. X-ray fiber pattern analysis, performed in this work on uniaxially drawn samples, revealed that crystallization of PBS at high supercooling of the melt causes the growth of crystals of low stability with an enlarged basal plane of the monoclinic unit cell and a lower crystal density compared to high-temperature crystallization. This finding is in line with widely observed crystallization-temperature-induced changes of the unit cell in many other polymers, pointing to the presence of conformational chain defects in crystals grown at relatively low temperatures.

© 2025 The Author(s). Macromolecular Chemistry and Physics published by Wiley-VCH GmbH

Supporting Information

Supporting Information is available from the Wiley Online Library or from the author.

Acknowledgements

The project was funded by the Deutsche Forschungsgemeinschaft (DFG, German Research Foundation)-Projektnummer 439920697. The authors thank MCPP Germany GmbH for providing the material.

Open access funding enabled and organized by Projekt DEAL.

Conflict of Interest

The authors declare no conflict of interest.

Data Availability Statement

The data that support the findings of this study are available from the corresponding author upon reasonable request.

Keywords

crystal structure, crystallization, disorder crystals, poly(butylene succinate), X-ray diffraction

Received: February 12, 2025
Revised: March 10, 2025
Published online: March 25, 2025

---

[1] S. Kato, T. Ueda, T. Aoshima, N. Kosaka, S. Nitta, *Adv. Polym. Sci.* **2023**, *293*, 269.
[2] J. Xu, B. H. Guo, *Biotechnol. J.* **2010**, *5*, 1149.
[3] M. Barletta, C. Aversa, M. Ayyoob, A. Gisario, K. Hamad, M. Mehrpouya, H. Vahabi, *Progr. Polym. Sci.* **2022**, *132*, 101579.
[4] L. Aliotta, M. Seggiani, A. Lazzeri, V. Gigante, P. Cinelli, *Polymers* **2022**, *14*, 844.
[5] O. Platnieks, S. Gaidukovs, V. K. Thakur, A. Barkane, S. Beluns, *Eur. Polym. J.* **2021**, *161*, 110855.
[6] F. Signori, M. Pelagaggi, S. Bronco, M. C. Righetti, *Thermochim. Acta* **2012**, *543*, 74.
[7] M. L. Di Lorenzo, R. Androsch, M. C. Righetti, *Eur. Polym. J.* **2017**, *94*, 384.
[8] J. J. Moura Ramos, H. P. Diogo, *Polym. Eng. Sci.* **2015**, *55*, 1873.
[9] T. Miyata, T. Masuko, *Polymer* **1998**, *39*, 1399.
[10] G. Z. Papageorgiou, D. N. Bikiaris, *Polymer* **2005**, *46*, 12081.
[11] Z. Gan, H. Abe, H. Kurokawa, Y. Doi, *Biomacromolecules* **2001**, *2*, 605.
[12] E. S. Yoo, S. S. Im, *J. Polym. Sci., Polym. Phys.* **1999**, *37*, 1357.
[13] K. J. Ihn, E. S. Yoo, S. S. Im, *Macromolecules* **1995**, *28*, 2460.
[14] H. Wang, J. M. Schultz, S. Yan, *Polymer* **2007**, *48*, 3530.
[15] H. Wang, Z. Gan, J. M. Schultz, S. Yan, *Polymer* **2008**, *49*, 2342.
[16] J. W. Park, D. K. Kim, S. S. Im, *Polym. Int.* **2002**, *51*, 239.
[17] C. Schick, A. Toda, R. Androsch, *Macromolecules* **2021**, *54*, 3366.
[18] R. Androsch, K. Jariyavidyanont, A. Janke, C. Schick, *Polymer* **2023**, *285*, 126311.
[19] K. Jariyavidyanont, C. Schick, R. Androsch, *Macromol. Rapid Comm.* **2024**, *45*, 2400273.
[20] M. Kakudo, N. Kasai, *X-Ray Diffraction by Polymers*, Elsevier, Amsterdam, Netherlands **1972**.
[21] Y. Ichikawa, H. Kondo, Y. Igarashi, K. Noguchi, K. Okuyama, J. Washiyama, *Polymer* **2000**, *41*, 4719.
[22] Y. Ichikawa, J. Suzuki, J. Washiyama, Y. Moteki, K. Noguchi, K. Okuyama, *Polymer* **1994**, *35*, 3338.
[23] Y. Ichikawa, J. Washiyama, Y. Moteki, K. Noguchi, K. Okuyama, *Polym. J.* **1995**, *27*, 1230.
[24] G. Natta, P. Corradini, *Il Nuovo Cimento* **1960**, *15*, 40.
[25] R. Androsch, M. L. Di Lorenzo, C. Schick, B. Wunderlich, *Polymer* **2010**, *51*, 4639.
[26] G. F. Schmidt, H. A. Stuart, *Zeitschrift für Naturforschung A* **1958**, *13*, 222.
[27] A. Ziabicki, *Kolloid-Zeitschrift* **1959**, *167*, 132.
[28] M. Rhoades, N. Wonderling, C. Schick, R. Androsch, *Polymer* **2016**, *106*, 29.
[29] M. Gohn, A. M. Rhoades, N. Wonderling, T. Tighe, R. Androsch, *Thermochim. Acta* **2017**, *655*, 313.
[30] J. Zhang, Y. Duan, H. Sato, H. Tsuji, I. Noda, S. Yan, Y. Ozaki, *Macromolecules* **2005**, *38*, 8012.
[31] J. Zhang, K. Tashiro, A. J. Domb, H. Tsuji, *Macromol. Symp.* **2006**, *242*, 274.
[32] K. H. Nitta, K. Odaka, *Polymer* **2009**, *50*, 4080.
[33] Q. Zia, H.-J. Radusch, R. Androsch, *Polym. Bull.* **2009**, *63*, 755.
[34] L. Shen, I. Y. Phang, T. Liu, *Polym. Test.* **2006**, *25*, 249.
[35] K. Jariyavidyanont, Q. Yu, A. Petzold, T. Thurn-Albrecht, R. Glüge, H. Altenbach, R. Androsch, *J. Mech. Behav. Biomed. Mater.* **2023**, *137*, 105546.
[36] K. Jariyavidyanont, C. Wüstefeld, T. Chudoba, R. Androsch, *Polym. Test.* **2024**, *137*, 108524.
[37] R. Androsch, A. M. Rhoades, I. Stolte, C. Schick, *Eur. Polym. J.* **2015**, *66*, 180.
[38] Product information MCPP Germany GmbH, https://www.mcpp-global.com/en/mcpp-english-europe/products/product/biopbsTM-general-properties/ (accessed: October **2024**).
[39] Personal communication with MCPP Germany GmbH (July/2019).
[40] W. G. Perkins, *Polym. Eng. Sci.* **1999**, *39*, 2445.
[41] T. Wang, H. Wang, H. Li, Z. Gan, S. Yan, *Phys. Chem. Chem. Phys.* **2009**, *11*, 1619.
[42] D. G. Papageorgiou, E. Zhuravlev, G. Z. Papageorgiou, D. Bikiaris, K. Chrissafis, C. Schick, *Polymer* **2014**, *55*, 6725.
[43] J. Jiang, E. Zhuravlev, W. B. Hu, C. Schick, D. S. Zhou, *Chin. J. Polym. Sci.* **2017**, *35*, 1009.
[44] R. Androsch, M. Stolp, H.-J. Radusch, *Acta Polym.* **1996**, *47*, 99.
[45] J. Grebowicz, S. F. Lau, B. Wunderlich, *J. Polym. Sci. Polym. Symp.* **1984**, *71*, 19.
[46] Z. G. Wang, B. S. Hsiao, S. Srinivas, G. M. Brown, A. H. Tsou, S. Z. D. Cheng, R. S. Stein, *Polymer* **2001**, *42*, 7561.
[47] D. S. Langhe, A. Hiltner, E. Baer, *J. Polym. Sci. Polym. Phys.* **2011**, *49*, 1672.
[48] J. Zhang, K. Tashiro, H. Tsuji, A. J. Domb, *Macromolecules* **2008**, *41*, 1352.
[49] R. Androsch, C. Schick, M. L. Di Lorenzo, *Macromol. Chem. Phys.* **2014**, *215*, 1134.
[50] J. P. Kalish, K. Aou, X. Yang, S. L. Hsu, *Polymer* **2011**, *52*, 814.
[51] M. C. Righetti, M. Gazzano, M. L. Di Lorenzo, R. Androsch, *Eur. Polym. J.* **2015**, *70*, 215.
[52] K. Jariyavidyanont, M. Du, Q. Yu, T. Thurn-Albrecht, C. Schick, R. Androsch, *Macromol. Rapid Comm.* **2022**, *43*, 2200148.
[53] K. Jariyavidyanont, C. Schick, R. Androsch, *Thermochim. Acta* **2022**, *717*, 179349.
[54] K. H. Illers, *Die Makromol. Chemie: Macromol. Chem. Phys.* **1978**, *179*, 497.

© 2025 The Author(s). Macromolecular Chemistry and Physics published by Wiley-VCH GmbH

15213935, 2025, 11, Downloaded from https://onlinelibrary.wiley.com/doi/10.1002/macp.202500079 by Martin Luther University Halle-Wittenberg, Wiley Online Library on [27/06/2025]. See the Terms and Conditions (https://onlinelibrary.wiley.com/terms-and-conditions) on Wiley Online Library for rules of use; OA articles are governed by the applicable Creative Commons License